https://doi.org/10.5194/tc-2021-193
Preprint. Discussion started: 16 July 2021

The Cryosphere Discussions
Open Access
EGU

Comparison of ice dynamics using full-Stokes and Blatter-Pattyn approximation: application to the central North East Greenland Ice Stream

Martin Rückamp[1], Thomas Kleiner[1], and Angelika Humbert[1,2]

[1]Alfred-Wegener-Institut Helmholtz-Zentrum für Polar- und Meeresforschung, Bremerhaven, Germany
[2]Faculty of Geoscience, University of Bremen, Bremen, Germany

Correspondence: Martin Rückamp (martin.rueckamp@awi.de), Angelika Humbert (angelika.humbert@awi.de)

Abstract. Full-Stokes (FS) ice sheet models provide the most sophisticated formulation of ice sheet flow. However, their applicability is often limited due to its high computational demand and its owing numerical challenges. To balance computational demand and accuracy, the so-called Blatter-Pattyn (BP) stress regime is frequently used. Here, we explore the dynamic consequences caused by solving FS and the BP stress regime applied to the central part of the North East Greenland Ice Stream (NEGIS). To ensure a consistent comparison, we use one single ice sheet model to run the simulations under identical numerical conditions. A sensitivity study to grid resolution reveals that velocity differences between the FS and BP solution emerge below ∼1 km horizontal resolution and continuously increases with resolution. Generally, BP produces higher surface velocities than FS, at a resolution of 0.1 km up to 5.8% on average. In an extreme case, estimated ice discharge rates are up to 8% overestimated by BP; in a rather classical case, BP reveals up to 3% more ice discharge. Based on these minor model disagreements and given other large uncertainties in ice sheet projections, we conclude that the use of FS seems not an urgent issue and takes a secondary role in narrowing uncertainties of current sea-level projections. However, the englacial advection schemes from both stress regimes indicate severe impacts on internal layers of ice sheets.

1 Introduction

The most comprehensive description of ice sheet flow is by using the full-Stokes (FS) equations. As no simplification to the equation system is made, such a model is considered the most accurate available, capable of describing highly dynamic ice sheets, including ice streams, ice shelves, and grounding line migration. But this formulation is also the most computationally intensive, both from the numerical perspective and because FS effects can only occur at higher resolutions compared to simpler models.

Due to increasing computer power, the emergence of new generation ice sheet models (ISMs) in the last decades allowed ice flow models with varying degrees of approximations to the Stokes equations or even with no approximation. Although

https://doi.org/10.5194/tc-2021-193
Preprint. Discussion started: 16 July 2021

ice dynamical processes require a most accurate representation of the stresses, e.g. in regions of high variability in basal topography and/or basal slipperiness (Gudmundsson, 2003; Hindmarsh, 2004), simplifications to FS are still necessary for e.g. long time integrations or for large ensemble modelling to keep the computing time affordable. For this reason, ice flow modelling has frequently relied on simplified mathematical models to balance computational costs and accuracy, such as the three-dimensional and computational efficient Blatter-Pattyn (BP) formulation. Although BP neglects severe components of the full system, it is considered valid in the majority of an ice sheet.

Under these conditions, current ice sheet projections within the ISMIP6 effort (Ice Sheet Model Intercomparison Project for CMIP6 (ISMIP6), Nowicki et al., 2016) cover a large diversity in model approaches and approximations to the Stokes flow (Goelzer et al., 2018; Seroussi et al., 2019; Goelzer et al., 2020; Seroussi et al., 2020), but only one contribution solved the FS problem (Seroussi et al., 2020). Up to now, there is no clear understanding of whether FS simulations have the potential in narrowing uncertainties in current sea-level predictions from the Greenland and Antarctic ice sheets. However, the fidelity to accurately simulate the behaviour of outlet glaciers has been cited in the reports of the Intergovernmental Panel on Climate Change as a prerequisite for reliable ice sheet projections (IPCC, 2013; Oppenheimer et al., 2019).

In earlier ISMIPs the performance in simulating idealized ice stream and marine ice sheet dynamics by ISMs was explored (ISMIP-HOM (Ice Sheet Model Intercomparison Project for Higher-Order Models, Pattyn et al., 2008), MISMIP2d (Marine Ice Sheet Model Intercomparison Project, Pattyn et al., 2012), MISMIP3d (Pattyn et al., 2013), MISMIP+ (Cornford et al., 2020)). ISMIP-HOM particularly reveals that the FS models show a much smaller spread, hence are in better agreement with one another and with the analytical solution. In the earlier MISMIP experiments, any systematic study of differences in solutions from Stokes models is prohibited due to the limited number of FS models[1]. The recent MISMIP+ effort reflects that the choice of the friction law plays a larger role compared to, e.g. ice flow approximations (two FS models contribute to this exercise). From these synthetic scenarios, it yet needs to be assessed if discrepancies between FS and simpler models are minor compared to other uncertainties in ice sheet modelling given the huge additional computational amount consumed by FS models.

In contrast to the idealized ISMIP experiments, the influence of FS on ice dynamical behaviour compared to simpler models were tested on realistic problems (e.g. Leysinger Vieli and Gudmundsson, 2004; Le Meur et al., 2004; Morlighem et al., 2010; Seddik et al., 2012; Favier et al., 2014; Seddik et al., 2017). These exercises provide important insights into the transient response and indicate that FS produces different results as simpler models. For example, in most of the conducted projection experiments, FS tends to contribute less to sea-level rise than simpler models under identical projection scenarios (Seddik et al., 2012; Favier et al., 2014; Seddik et al., 2017). However, assessing whether FS is urgently needed compared to simpler models is complicated because of many interacting processes: (i) comparability is often limited by the use of different ISMs as it is not entirely clear how much of the differences is due to numerical treatments as, e.g. different grids, which resolves, e.g. bed differently, or discretization schemes. (ii) Differences are also subject to e.g. assumptions in basal flow conditions or the initialization approach. (iii) Moreover, when transient simulations are forced with climate scenarios, the response involves numerous processes and interactions that makes it difficult to separate causes.

[1]Compared to the ISMIP-HOM experiments, the MISMIP experiments require a long transient integration, which is costly to perform for an FS model.

https://doi.org/10.5194/tc-2021-193
Preprint. Discussion started: 16 July 2021

The Cryosphere Discussions
Open Access
EGU

Beside the relevance of utilizing FS or simpler models for future projections of ice sheets, the different ice dynamics may have a severe impact on the internal ice flow. The internal ice flow computed by ISMs are used to estimate the englacial layering (e.g., Born, 2017) which can further serve as tuning targets for paleoclimatic simulations (e.g., Sutter et al., 2020). The effect on how different flow approximations affect the internal architecture of ice sheets have received so far no attention to our knowledge; certainly because FS and higher-order models are too expensive for these long-time integrations.

Here, we intend to overcome model-intercomparison shortcomings by performing a consistent analysis of differences in stress and velocity fields solving the FS system or using the Blatter-Pattyn (BP) approximation (Blatter, 1995; Pattyn, 2003). Our comparison focuses on FS to BP, as the latter is more frequently used as a compromise between computational costs and accuracy. The employed ISM, namely COMice (Wilkens et al., 2015), includes the option to run the FS model or to activate the BP mode allowing us to compare the results consistently as they are computed under the same numerical conditions. Here, we strive to fill the gap of FS and BP intercomparisons in synthetic scenarios towards a high-resolution real system application. Therefore, we select a subset of the North East Greenland Ice Stream (NEGIS) as an investigation area. The subset covers slow and fast flowing ice as well as a smooth and higher variable bed topography. Our study is not based on the transient behaviour, we rather aim to address ice dynamical differences between the stress regimes. However, from the simulated 3D ice flow we discuss potential consequences for capturing englacial layers utilizing different flow approximations. As differences between FS and BP are expected to emerge in regions with steep bed gradients or high aspect ratios (height/length ratio), we step-wise increase spatial resolution from 12.8 km down to a resolution of 0.1 km. In order to investigate whether differences are controlled by the slip ratio (ratio between basal sliding and gravitational driven flow) the ice stiffness is weighted by the enhancement factor.

2 Theoretical background

2.1 Field equations

The core of the FS equation system builds the momentum (neglecting acceleration) and mass balance equation for incompressible ice and is written as

$$\operatorname{div} \mathbf{t} = \varrho_i \boldsymbol{g}, \tag{1}$$

$$\operatorname{div} \boldsymbol{v} = 0, \tag{2}$$

with the density of ice ϱ_i, the three dimensional velocity field $\boldsymbol{v} = (v_x, v_y, v_z)$ in Cartesian coordinates, the gravitational acceleration vector pointing downward $\boldsymbol{g} = -g\boldsymbol{e}_z$, and the Cauchy stress tensor $\boldsymbol{t}$. We split the Cauchy stress into a deviatoric part $\mathbf{t}^{\mathrm{D}}$ and an isometric pressure p

$$\mathbf{t} = \mathbf{t}^{\mathrm{D}} + p\boldsymbol{I}, \tag{3}$$

https://doi.org/10.5194/tc-2021-193
Preprint. Discussion started: 16 July 2021

The Cryosphere
Discussions
Open Access
EGU

with $p = -\frac{1}{3}\mathrm{tr}(\mathbf{t})$ and $\boldsymbol{I}$ the identity tensor. The constitutive equation for the non-Newtonian fluid is given by the Glen-Steinemanns flow law (Glen, 1955; Steinemann, 1954)

$$\mathbf{t}^{\mathrm{D}} = 2\eta \boldsymbol{D}, \tag{4}$$

where $\boldsymbol{D}$ is the strain rate tensor and links strain rates to the symmetric part of the velocity gradients ($\boldsymbol{D} = \frac{1}{2}(\mathrm{grad}\,\boldsymbol{v} + (\mathrm{grad}\,\boldsymbol{v})^T)$). The viscosity is defined as

$$\eta = \frac{1}{2} E A(T,W)^{-1/n} \dot{\varepsilon}_e^{(1-n)/n}, \tag{5}$$

with the flow law exponent n, the enhancement factor E, the rate factor A depending on temperature T and microscopic water content W, and the effective strain rate $\dot{\varepsilon}_e$ being the second invariant of the strain-rate tensor. To the latter, a small value of $\dot{\varepsilon}_0 = 10^{-30}\,\mathrm{s}^{-1}$ is added to keep the term non-zero.

2.2 Boundary conditions

Boundary condition at the upper surface is traction-free. The ice sheet base is subject to basal sliding according to a friction law for the basal shear stress $\boldsymbol{t}_{\mathrm{b}}^{\mathrm{D}}$ in the tangential plane

$$\boldsymbol{t}_{\mathrm{b}}^{\mathrm{D}} = [(\boldsymbol{I} - \boldsymbol{n}\boldsymbol{n}^T)\boldsymbol{t}^{\mathrm{D}}] \cdot \boldsymbol{n} = -\beta^2 (\boldsymbol{I} - \boldsymbol{n}\boldsymbol{n}^T) \cdot \boldsymbol{v} = -\beta^2 \boldsymbol{v}_{\mathrm{b}}, \tag{6}$$

$$\boldsymbol{v} \cdot \boldsymbol{n} = 0, \tag{7}$$

with the unit normal vector $\boldsymbol{n}$ pointing outwards of the ice, and $\boldsymbol{v}_{\mathrm{b}}$ the velocity in the tangential plane at the base. Basal refreezing or melting is neglected. The basal drag parameter β^2 usually includes the effective pressure to account for the presence of water lubricating the ice-bed interface, as well as bed properties such as roughness. The parameterization for β^2 and the remaining lateral boundary condition are given below for each experiment setup.

2.3 Model classification

The momentum balance (Eq. 1) can be written in terms of velocity components and pressure p

$$\begin{aligned}
&\frac{\partial}{\partial x}\left(2\eta\frac{\partial v_x}{\partial x}\right) + \frac{\partial}{\partial y}\left(\eta\frac{\partial v_x}{\partial y} + \eta\frac{\partial v_y}{\partial x}\right) + \frac{\partial}{\partial z}\left(\eta\frac{\partial v_x}{\partial z} + \eta\frac{\partial v_z}{\partial x}\right) - \frac{\partial p}{\partial x} = 0,\\
&\frac{\partial}{\partial x}\left(\eta\frac{\partial v_x}{\partial y} + \eta\frac{\partial v_y}{\partial x}\right) + \frac{\partial}{\partial y}\left(2\eta\frac{\partial v_y}{\partial y}\right) + \frac{\partial}{\partial z}\left(\eta\frac{\partial v_y}{\partial z} + \eta\frac{\partial v_z}{\partial y}\right) - \frac{\partial p}{\partial y} = 0,\\
&\frac{\partial}{\partial x}\left(\eta\frac{\partial v_x}{\partial z} + \eta\frac{\partial v_z}{\partial x}\right) + \frac{\partial}{\partial y}\left(\eta\frac{\partial v_y}{\partial z} + \eta\frac{\partial v_z}{\partial y}\right) + \frac{\partial}{\partial z}\left(2\eta\frac{\partial v_z}{\partial z}\right) - \frac{\partial p}{\partial z} = -\varrho_i g,
\end{aligned} \tag{8}$$

as well as the effective strain rate occurring in Eq. 5

$$\dot{\varepsilon}_e = \left(\frac{1}{2}\left(\left(\frac{\partial v_x}{\partial x}\right)^2 + \left(\frac{\partial v_y}{\partial y}\right)^2 + \left(\frac{\partial v_z}{\partial z}\right)^2\right) + \frac{1}{4}\left(\frac{\partial v_x}{\partial y} + \frac{\partial v_y}{\partial x}\right)^2 + \frac{1}{4}\left(\frac{\partial v_x}{\partial z} + \frac{\partial v_z}{\partial x}\right)^2 + \frac{1}{4}\left(\frac{\partial v_y}{\partial z} + \frac{\partial v_z}{\partial y}\right)^2\right)^{1/2}. \tag{9}$$

https://doi.org/10.5194/tc-2021-193
Preprint. Discussion started: 16 July 2021

The red terms are omitted in the BP approximation explained below. The four equations (Eqs. 2 and 8) with the four unknowns v_x, v_y, v_z and p are forming the FS equation system. Various approximations to this set of equation exist ranging from shallow ice to different types of one layer and multilayer approximations for non-horizontal shear components of the stress tensor (Hutter, 1983; Hindmarsh, 2004; Bueler and Brown, 2009; Ahlkrona et al., 2013). The FS problem has saddle point character which is difficult to solve. In order to reduce the computational demand and derive a better posed problem, Blatter (1995) and Pattyn (2003) developed the so-called BP approximation scheme which is valid for most of the ice sheet domain and up-to-date widely used in ice flow models. The main assumption of their model is that the vertical component of the momentum balance is approximated as hydrostatic (i.e. $\partial t_{zz}/\partial z = \varrho_i g$). This is used to eliminate the pressure variable p from the FS equation system and reduces the FS problem with the two horizontal velocity components as unknown field variables. The further assumption that horizontal gradients of the vertical velocity are small compared to the vertical gradient of the horizontal velocity (i.e. $\partial v_z/\partial x \ll \partial v_x/\partial z$ and $\partial v_z/\partial y \ll \partial v_y/\partial z$) leads to a closed problem for the two horizontal velocity components. This approximation is equivalent to dropping the red coloured terms in Eq. 8 and 9; it is termed LMLa in Hindmarsh (2004).

The simplifications made by BP on the FS system reduces the computational demand by deriving a better posed problem. By re-arranging the BP equations this system leads to a closed problem for the two horizontal velocity components v_x and v_y. In doing so, the BP approximations decouple the vertical velocity v_z and the pressure p from the full system. Both unknowns are recovered diagnostically by integrating the incompressibility equation (Eq. 2) and the vertical component of the momentum balance equation (Eq. 8), respectively. However, in our approach we are following an alternative way to realize the BP stress regime (see Sect. 3.1 and 3.2).

3 Model description and verification

3.1 Ice flow model

To solve the set of equations presented above (Eq. 1, 2 and boundary conditions), we use the COMmercial finite element SOLver (COMSOL) Multiphysics© (version 5.5, www.comsol.com, last access May 2021). COMSOL provides a FS interface which is additionally manipulated in order to realise the BP stress regime. This is accomplished by discarding the corresponding terms (red terms in Eqs. 8 and 9) in the weak formulation but maintaining identical FS numerical details. That means that the BP stress regime does not further modify the default FS module, i.e the BP version implemented in this study is not forming a multilayer model with the two horizontal velocity components as field variables. Therefore, our implemented BP approximation is hereafter termed BP-like. In doing so, both flow modes (FS and BP-like) are running through the same (FS) solving algorithm. Hereby we ensure that differences in the computed results due to numerical issues are eliminated. However, the disadvantage is that we do not benefit by the reduced complexity of the BP approximation. As a consequence of the avoided decoupling, $\partial v_z/\partial z$ in Eq. 9 is not replaced by $-(\partial v_x/\partial x + \partial v_y/\partial y)$ as commonly done in HO approximations (e.g. Pattyn, 2003).

https://doi.org/10.5194/tc-2021-193
Preprint. Discussion started: 16 July 2021

3.2 Numerics

The mass balance and momentum equations constitute a nonlinear equation system. Independent of the employed flow regime, a damped Newton method (which is COMSOL's default solver) is applied in a fully coupled manner to solve for the velocity vector $\boldsymbol{v}$ and the pressure p. The unstabilized Stokes equation (Eq. 8) is subject to the Babuska-Brezzi condition, which states that the basis functions for p have to be of lower order than for $\boldsymbol{v}$. As we stabilize the FS equation with streamline diffusion (Galerkin least-squares (GLS), Hauke and Hughes, 1994) it is possible to use equal-order interpolation to keep the computational amount limited; i.e. linear elements for both the velocity components and the pressure field (P1+P1 Lagrange elements).

All flow regime equations are forming a saddle point problem, for which either a direct solver or special preconditioning is needed. The verification tests ISMIP-HOM (see Sect. 3.3) are solved with the direct solver MUMPS (https://graal.ens-lyon.fr/MUMPS/; last access August 2020). For the NEGIS subset experiment (Sect. 4), the degrees of freedom (DOF) increases rapidly with increasing spatial resolution, and a direct solver would be uncommon for such large numbers of DOFs. However, the smaller problems are solved with the direct solver MUMPS, while for the higher resolutions we rely on a Domain Decomposition solver with an overlapping additive Schwarz method (ASM, Widlund and Toselli, 2005) which is much superior in terms of the required computation time and working memory. ASM is a memory-efficient and scalable iterative algorithm for large problems, to accelerate the iterative GMRES solver (Saad, 2003). Very briefly, the solution is found by iteratively solving each subdomain problem with all other domains fixed until convergence is achieved. In each subdomain, the boundary condition is taken from neighbouring subdomains. The employed overlapping method is a multiplicative Schwarz method. The multiplicative method solves each subdomain problem in sequence and might be not suitable for running in parallel. But it reveals much faster convergence and lower memory consumption than other overlapping methods available in COMSOL (symmetric, additive and hybrid).

In terms of the stressed consistency between the simulations results, we must clarify the different usage of the linear solvers: the coarser models show a poor performance with the ASM solver. At the same time, the higher resolutions run out of memory with the MUMPS solver. But the limiting case with a horizontal grid resolution of l=0.4 km reveals differences between MUMPS and ASM results well below $10^{-7}\,\mathrm{m\,a^{-1}}$ in the surface velocity. Consequently, we assume that both applied solvers provide comparable results.

3.3 Verification by benchmarks

The ISMIP-HOM benchmark targets comparison for three dimensional ice flow models arising from basal topography undulations, from basal sliding and by changing the length scale. From the ISMIP-HOM setup (Pattyn et al., 2008) we select the 3D and non-transient experiments Exp. A (Ice flow over a bumpy bed) and Exp. C (Ice stream flow I). We rely on this setup to verify our flow implementations, in particular the BP-like implementation. Please note that the FS implementation is basically verified by the 'mmr' contribution to Pattyn et al. (2008) but is based on COMSOL version 3.5. Exp. A is a parallel-sided slab with a series of sinusoidal oscillations in the basal topography with a frequency of $\omega = 2\pi/L$, with L being the domain length.

https://doi.org/10.5194/tc-2021-193
Preprint. Discussion started: 16 July 2021

Exp. C is parallel-sided slab with a series of sinusoidal oscillations on the basal drag parameter β^2 (Eq. 6) with the frequency ω. At the lateral margins periodic boundary conditions are applied. The length scale is subsequently reduced as L =160, 80, 40, 20, 10 and 5 km so that full-Stokes effects can develop due to the higher aspect ratio H/L, with H being the ice thickness. The domain is discretized with $n_x = n_y = L/41$ grid points in the horizontal plane. In the vertical direction 15 layers refined to the base are chosen. The parameters and constants used in this setup are listed in Tab. 1. For a detailed description of the experimental setup, please refer to Pattyn et al. (2008).

Our results for FS and BP-like show good agreements with corresponding models for FS and non FS (nFS; nFS includes BP) for the conducted A and C test cases (see Appendix Figs. A3 and A4). However, the original exercise reveals distinct differences between FS and lower order approximations on short length scales. On those, different characteristics between FS and HO emerge (Fig. 1). In particular, for Exp. C the 'double-peak' in the surface velocity is present in the FS solution but absent in the BP regime, which is consistent with the original ISMIP-HOM results. From the resulting behavior, the implementations of the FS and BP-like stress regimes are verified.

4 Description of NEGIS subset experiment

We select a subset of the NEGIS (Fig. 2) to investigate the effect of FS and BP on its ice dynamics. This region comprises abrupt changes in slow and fast flow suitable to conduct such an analysis. On purpose, a region far upstream the grounding line and far downstream the ice divide is selected to avoid grounding line treatment and to focus on an ice-stream like flow regime. The geometry of the NEGIS subset is laterally defined along flow lines that were deduced from the MEaSUREs surface velocity data-set (Joughin et al., 2016, 2018). Bed and surface topography are taken from BedMachine v3 (BM, Morlighem et al., 2017).

In the NEGIS experiment we consider a Budd-like friction type (Budd et al., 1979) with a linear relationship on the effective pressure, N. The basal drag parameter β^2 in the basal boundary condition (Eq. 6) is assumed as

$$\beta^2 = k^2 N, \tag{10}$$

where k is the basal friction coefficient. The effective normal pressure is the difference between the local normal stress on the bed boundary P_i and the basal water pressure P_w

$$N = P_\mathrm{i} - P_\mathrm{w}. \tag{11}$$

The basal water pressure is computed in marine parts, i.e. where the ice base is below the sea-level ($h_b < z_\mathrm{sl}$), according to Huybrechts (1992)

$$P_\mathrm{i} = -(\boldsymbol{t}\cdot\boldsymbol{n})\cdot\boldsymbol{n}, \tag{12}$$

$$P_\mathrm{w} = -\min(\varrho_\mathrm{w} g h_\mathrm{b}, 0), \tag{13}$$

where ϱ_w is the density of the ocean and h_b the bed elevation. Independent of the employed stress regimes the ice pressure P_i is the normal stress instead of the approximated ice overburden pressure. The assumptions made about the water pressure

https://doi.org/10.5194/tc-2021-193
Preprint. Discussion started: 16 July 2021

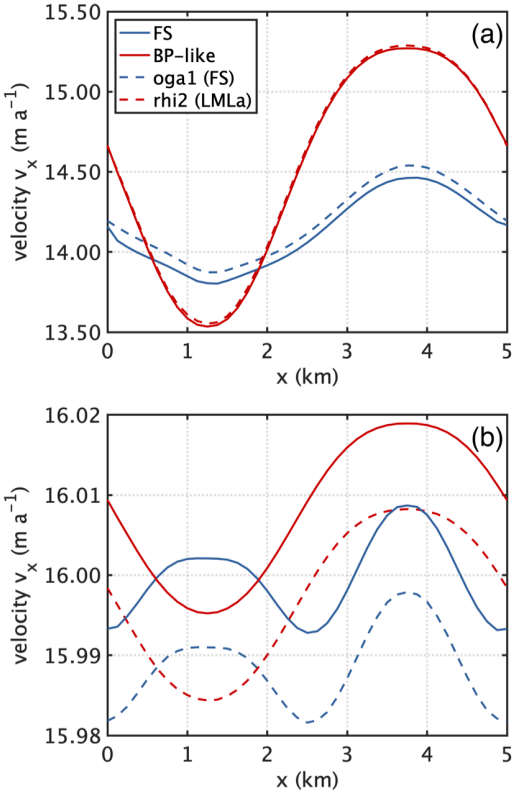

Figure 1. Results of the ISMIP-HOM experiments A (a) and C (b) for the length scale $L = 5\,\mathrm{km}$. Surface velocity component v_x ($\mathrm{m\,a^{-1}}$) at $y = L/4$. Values computed in this study for FS and BP-like are compared to the BP model 'rhi2' and the FS model 'oga1' from the original ISMIP-HOM benchmark (Pattyn et al., 2008). Please note that the BP-like and BP solutions in Exp. A overlay each other.

imply that the base is perfectly connected to the ocean at any location in the domain that is below sea-level. Overall, this might be incorrect but it forms an appropriate assumption in the absence of an additional hydrological model.

Solving a subset of an ice stream poses unknown boundary conditions in the interior of the ice sheet. A very simple approach would be prescribing the measured surface velocities as a depth-averaged velocity profile. However, we choose boundary conditions that are free to adjust during the solution process. Laterally boundary conditions are chosen to have a symmetry boundary condition at the inflow boundary, free slip at lateral along-flow boundaries and a normal stress condition at the outflow boundary with $\boldsymbol{t} \cdot \boldsymbol{n} = \varrho_i g(z_s - z)$, where z_s is the surface elevation and z the vertical coordinate.

https://doi.org/10.5194/tc-2021-193
Preprint. Discussion started: 16 July 2021

The Cryosphere Discussions
Open Access
EGU

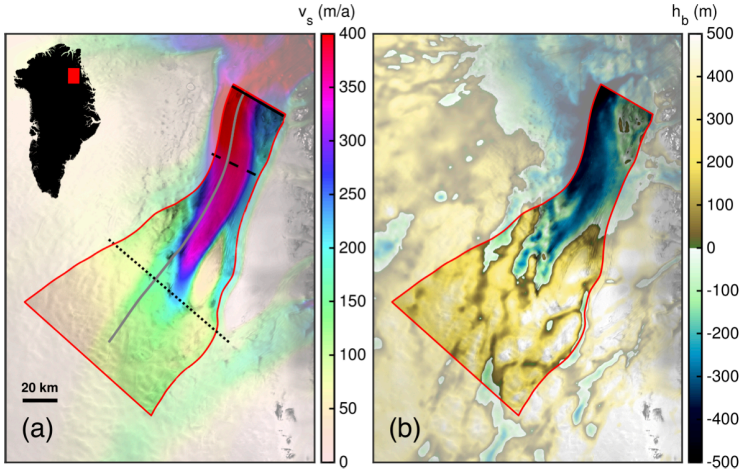

Figure 2. Overview of the NEGIS region and modelling domain. (a) Observed surface velocities (Joughin et al., 2016, 2018). (b) Bed topography (Morlighem et al., 2017). The red line in (a) and (b) delineates the modelling domain. In (a), the black lines (dotted, dashed, straight) indicate fluxgate locations (see Fig. 10 and related text below) and the grey line the pathway of seeded particles (see Fig. 9 and related text below). Background image is a RADARSAT Mosaic (Joughin, 2015; Joughin et al., 2016)

We conduct experiments with different horizontal mesh resolutions $l = 12.8$, 6.4, 3.2, 1.6, 0.8, 0.4, 0.2, 0.15 and 0.1 km. Please note, that $l = 0.15$ km is the nominal resolution of the BM data-set. The horizontal grid sizes comprise resolutions currently used in ice sheet projections (e.g. Aschwanden et al., 2019; Goelzer et al., 2020; Seroussi et al., 2020) and beyond. In the vertical direction 11 layers (refined to the base) are employed which is sufficient compared to higher resolutions (Fig. A2). The 3D meshes comprise between 1960 and 32 864 970 prism elements, respectively, resulting in 5280 to 72 416 740 DOF for the mesh cases (Tab. 2). In addition, the enhancement factor in Eq. 5 is varied by $E = 0.1$, 1, 3, and 6. This weighting is used to investigate whether simulation differences stem from basal sliding (small E) or internal velocity (large E) and serve mainly as an intercomparison study for both model versions. In the following $E = 1$ will be referred as the 'classical case'. The upper and lower values of E are very extreme and likely do not reflect a realistic situation.

For the parameters $A(T, W)$ (Eq. 5) and k^2 (Eq. 10) we utilize external products and capacities:

1. To rely on a realistic thermal state but avoiding an intensive thermal spin-up run, we make use of an enthalpy field from a paleo-climatic spin-up with the ice sheet model SICOPOLIS (Rückamp et al., 2019) which is bilinearly interpolated to the COMSOL meshes. The temperature-dependent part of the rate factor in Eq. 5 for cold ice is computed by Cuffey and Paterson (2010), and the water-content-dependent part for temperate ice is by Lliboutry and Duval (1985).

2. We make use of the inversion capability in the Ice-sheet and Sea-level System Model (ISSM, Larour et al., 2012) to obtain a spatially varying basal friction coefficient k^2 (Fig. A1, see Appendix A). The ISSM inversion is performed with

https://doi.org/10.5194/tc-2021-193
Preprint. Discussion started: 16 July 2021

The Cryosphere Discussions
Open Access
EGU

Table 1. Constants and model parameters used within the NEGIS subset experiment.

Quantity	Value	Units
Seconds per year, spy	31536000	$\mathrm{s\,a^{-1}}$
Gravitational acceleration, g	9.81	$\mathrm{m\,s^{-2}}$
Ice density, ϱ_i	917	$\mathrm{kg\,m^{-3}}$
Ocean water density, ϱ_w	1023	$\mathrm{kg\,m^{-3}}$
flow law exponent, n	3	-

$l = 1\,\mathrm{km}$, with BP and for the individual E values. Similarly, the SICOPOLIS temperature field is interpolated to the 3D ISSM mesh. Subsequently, the inferred fields for k^2 are bi-linear interpolated to the COMSOL meshes.

It is worth to mention that the computational work by the BP-like model is not reduced compared to FS in our approach, whereas other ice sheet codes benefit highly from reduced cost for BP implementations. Overall, computational times varied between a few seconds towards several hours. A broad overview of consumed computational resources is given in Tab. 2. Further parameters and constants used in this setup are listed in Tab. 1.

5 Results of the NEGIS subset experiment

5.1 Overview of simulations results

An overview of input parameters and FS simulation results of the NEGIS subset are compared exemplary for $l = 6400\,\mathrm{m}$ and $100\,\mathrm{m}$ in Fig. 3. The slope of the bed and surface topography (Fig. 3a–f) and the friction coefficient (Fig. 3c, g) of the finer resolution reveals more small scale features and stronger amplitudes; particularly a rapidly varying bed and surface slope in the finer resolution. Despite both compared resolutions relying on the same inferred basal friction coefficient and input geometry, the interpolation to the computational grids produces striking differences. As a consequence the simulated surface velocity fields differ quantitatively (Fig. 3d, h). Both resolutions reproduce the NEGIS ice stream to some degree but the finer resolution features an extended fast flow region ($\gtrsim 350\,\mathrm{m\,a^{-1}}$) and more pronounced shear margins (i.e. sharper velocity gradients). As the ISSM simulations inferring the friction coefficient are conducted with a 1 km horizontal grid resolution and with the BP ice flow approximation, the COMSOL results among all applied resolutions and flow regimes are not excepted to perfectly match the observed velocity field. The purpose of the transferred friction coefficient from the ISSM inversion to COMSOL is to roughly reproduce the observed NEGIS flow pattern. A better fit to observations could be certainly achieved by performing the inversion for each setting separately; however, our experiments are designed to focus on stress regime inter-comparisons and not on an assessment to observations.

https://doi.org/10.5194/tc-2021-193
Preprint. Discussion started: 16 July 2021

Table 2. Overview of mesh characteristics and consumed computational resources. Number for non-linear iterations (damped Newton's method), computational time, and physical RAM usage are exemplary listed for $E = 0.1$ and FS; values do not vary much among other E and stress regimes settings. Solver and cluster settings (OpenMP (OMP) shared-memory threads and distributed-memory tasks (MPI)) are maintained identical between each resolution and stress regime. Computational time includes the solver procedure (e.g. assembling the stiffness matrix, load vector) and outside routines (e.g. construction of mesh, saving results). Generally, COMSOL is run in hybrid mode, that means the process is distributed to a user-defined number of OMP threads and MPI tasks. Without testing the performance thoroughly we achieve a good performance by OMP parallelism per physical node and MPI communication between physical nodes (the code is simply run in OMP mode if MPI is equal to one). The listed RAM usage refers to one MPI task. Please note, that the cluster settings (MPI and OMP) have been chosen in a way that the job returns a solution within the cluster 'wall-time' but do not indicate any performance scaling.

resolution (km)	#elements	#DOF	lin-Solver	#non-lin iterations	time (minutes)	RAM (GB)	MPI I OMP
12.8†	1960	5280	MUMPS	11	0.11	1.87	1 I 36
6.4†	8560	20680	MUMPS	10	0.48	2.24	1 I 36
3.2†	32700	75548	MUMPS	9	1.72	4.03	1 I 36
1.6†	128530	289960	MUMPS	9	2.99	4.80	4 I 36
0.8†	512640	1142108	MUMPS	9	15.22	12.29	4 I 36
0.4†	2066130	4573976	ASM*	10	86.50	28.91	24 I 18
0.2†	8220400	18141816	ASM*	10	248.75	46.95	24 I 9
0.15†	14556150	32099408	ASM*	11	320.75	47.15	56 I 6
0.1‡	32864970	72416740	ASM*	11	708.11	359.60	30 I 48

† Simulations are run on the AWI cluster Cray CS 400. Each production node is equipped with 64 GB RAM and 2x18-Core CPUs (Intel Xeon Broadwell CPU E5-2697).
‡ Simulations are run at the North-German Supercomputing Alliance (HLRN) cluster Lise. Each production node is armed with 362 GB and 2x48-Core CPUs (Intel Cascade Lake Platinum 9242 (CLX-AP).
* Domain Decomposition solver with an overlapping multiplicative Schwarz method. Number of sub-domains are set equally to the number of MPI tasks.

5.2 Spatial differences between FS and BP-like

In the following, the FS solution is considered as the exact solution. Therefore, our analysis builds on presenting differences of the BP-like solution to FS. The differences of surface velocities, $v_s = |\boldsymbol{v}|$, between FS and BP-like are displayed for the 100 m grid resolution in Fig. 4 (differences for a resolution of 800 m and 6400 m are shown in Fig. A5). Spatial differences reveal a different patterns among the E values. For stiffer ice ($E = 0.1$) the BP-like solutions exhibits higher flow speeds which is almost confined to the fast flow region (Fig. 4a); this area partly coincides with a smooth bed and surface topography (see Fig. 3). Overall, discrepancies between FS and BP-like increase with higher velocities (scatter plot in Fig. 4a). The largest impact of BP-like on the solution is by enhancing the surface flow velocities up to 43 m a^{-1} compared to FS. For the 'classical case' ($E = 1$) the pattern is similar but with reduced magnitudes. In this setup, the BP-like velocities are up to 19 m a^{-1} higher. With softer ice ($E > 1$), the pattern in surface velocity differences changes and, eventually, for very soft ice ($E = 6$) differences are more pronounced in regions with higher topographic variability (compare Fig. 3) and exhibits a rippled pattern. Velocity

https://doi.org/10.5194/tc-2021-193
Preprint. Discussion started: 16 July 2021

The Cryosphere Discussions
Open Access
EGU

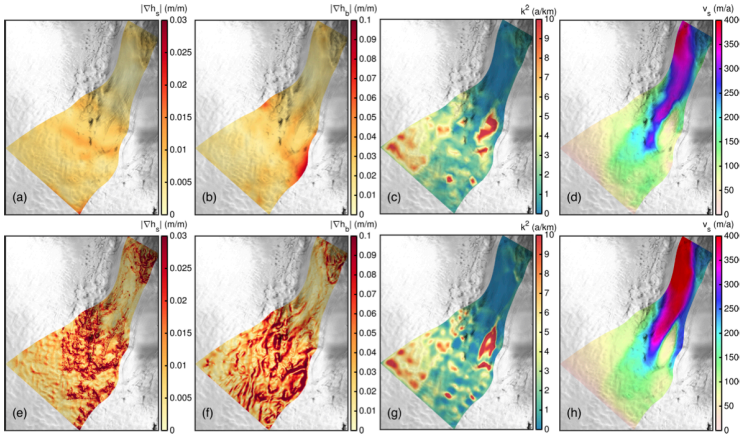

Figure 3. Overview of input parameters and exemplary simulation results of the NEGIS subset. Upper row shows slope of ice surface (a), slope of bed topography (b), basal friction coefficient for $E = 1$ (c), and simulated surface velocity with FS and $E = 1$ (d) for 6400 m horizontal resolution. Lower rows shows the same fields but for 100 m horizontal resolution. Background image is a RADARSAT Mosaic (Joughin, 2015; Joughin et al., 2016).

260 differences are scattered around the FS solution by $\pm 80\,\mathrm{m\,a^{-1}}$; the spread in differences is much stronger for softer ice (see scatter plots in Fig. 4).

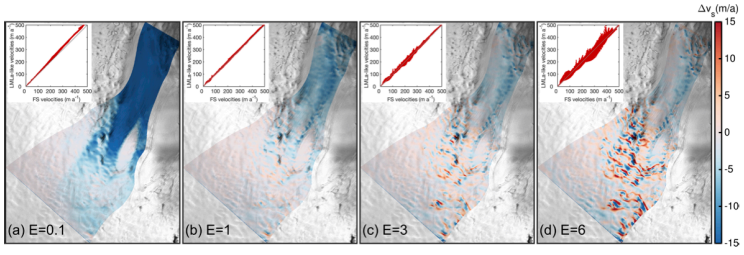

Figure 4. Difference of surface velocity $\Delta v_s^{\mathrm{FS-BP\text{-}like}} = v_s^{\mathrm{FS}} - v_s^{\mathrm{BP\text{-}like}}$ for a resolution of 100 m. (a, b, c, d) shows differences for $E = 0.1$, 1, 3 and 6, respectively. Background image is a RADARSAT Mosaic (Joughin, 2015; Joughin et al., 2016).

5.3 Integrative differences between FS and BP-like

Based on the spatial differences, we compute a spatially-averaged surface velocity, $v_s = |\boldsymbol{v}|$, for all parameter settings to obtain an integrative overview (Fig. 5). The analysis generally unveils that both the absolute spatially-averaged surface velocity

https://doi.org/10.5194/tc-2021-193
Preprint. Discussion started: 16 July 2021

The Cryosphere
Discussions
Open Access
EGU

(Fig. 5a–d) and relative spatially-averaged surface velocity differences (Fig. 5e–h) start to diverge somewhere below 1.6 and 0.8 km horizontal grid resolution (which is in the range of the mean ice thickness of 1330 m). Away from this threshold towards finer resolutions, solution differences show increasing trends between the stress regimes. For the finer resolutions BP-like produces higher mean surface velocities compared to FS. At the finest resolution (below the nominal resolution of the BM data-set), the mean velocity seem to reach a converged state for the BP-like stress regime (less pronounced for $E = 0.1$), but FS reveals a small dip towards lower velocities. The tendency of the diverging relative differences at the finest resolution is therefore likely a result from the still changing FS solution under grid refinements. The obtained tendency below 150 m is intriguing as the differences solely arise from grid-refinements and not due to the input geometry.

Maximum differences between FS and BP-like are obtained for the stiff-ice case ($E = 0.1$). The spatially-averaged ice flow velocity difference is up to $7\,\mathrm{m\,a^{-1}}$ for $E = 0.1$; the relative error between FS and BP-like is up to $\sim 5.8\%$. The resulting difference for $E = 1$ shows the same trend but is of lower magnitude (up to $\sim 1.5\%$). With softer ice ($E > 1$) the differences decrease. Interestingly, both stress regimes reveal an intermediate peak in mean surface velocity at $l = 1600\,\mathrm{m}$ over all E values.

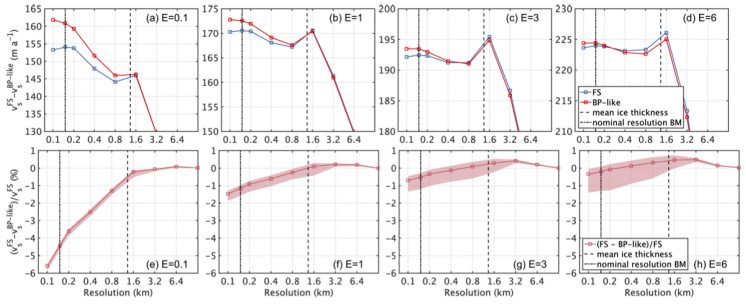

Figure 5. Integrative overview of spatially averaged surface velocities from FS and BP-like stress regimes. Upper row (a, b, c, d) shows surface velocity mean for $E = 0.1$, 1, 3, and 6, respectively. Lower row (e, f, g, h) shows the relative difference of BP-like to FS for or $E = 0.1$, 1, 3, and 6, respectively. The lighter background indicates the local maximum and minimum relative difference. Please note the logarithmic scale of the x-axis and the different scale of the y-axis in the upper row.

5.4 Relevant physical processes

The reasons for the disagreement in stress regime solutions are a complex composition of how ice dynamic processes are resolved, such as the basal boundary condition and the internal deformation. In addition, basal drag is coupled to internal deformation via the effective viscosity, making it difficult to separate the two entangled processes. Nevertheless, we strive to give a flavour of the origins by analyzing key processes of ice dynamics.

Figure 6a–d shows the difference of the basal velocity. Compared to the surface velocity differences, the softer ice shows a rather similar pattern. With softer ice, the accordance of the surface velocity difference pattern to the basal velocity difference

https://doi.org/10.5194/tc-2021-193
Preprint. Discussion started: 16 July 2021

pattern reduces. Most striking, the spread in velocity differences obtained at the ice surface for $E = 6$ is not evident at the ice base (compare scatter plots in Fig. 4d and 6d).

First of all we would expect, that FS would lead to larger ice velocities than BP due to the effective deformation rate (Eq. 9). FS captures the entire stress tensor, which is equivalent to making ice softer on average for the same flow parameters (assuming that strain-rate components shared by FS and BP-like have the same magnitude). Indeed, the depth-averaged viscosity, $\bar{\eta}$, is basically lower for FS compared to BP-like (Fig. 6i–l). For $E = 0.1$ the depth-averaged viscosity is lower at some larger areas, while for $E = 6$ the pattern changes towards several smaller patches; the magnitude of $\bar{\eta}$ among the E values changes by one order.

However, since FS generally reveals lower velocities than BP-like, the softer ice in FS appears to be levelled out by another process. A fundamental control on ice flow is the basal drag indicating the glacier's behaviour for fast flow. The spatial differences of basal drag inferred from the two models reveal that the basal drag is in the majority larger for FS compared to BP. This spatial pattern generally coincides with the obtained differences in surface velocity (Fig. 4a). For $E = 0.1$ the difference is largest (up to 140 kPa between FS and BP-like). In this setup, it seems that the basal drag is an essential control of the ice flow. With softer ice, the difference in the basal drag decreases.

Inspired by the findings of Gudmundsson (2003) and Hindmarsh (2004) deduced in idealized setups, we explore whether their derived criteria for an invalid BP solutions (BP invalid in regions of high slip ratio, high aspect ratio and high topographic variations) hold in our realistic setup. In Fig. 7 we present two-dimensional histograms of the relative velocity difference between FS and BP-like to the bed slope, $|\nabla h_b|$, to the local aspect ratio, H/l and to the FS slip ratio v_b/v_s (detailed line plots are in the Appendix Figs. A6, A7, A8, A9). Model differences emerge with increasing aspect ratio. Similarly, the error between FS and BP occurs in regions with high slip ratio (i.e near-plug-flow conditions prevail) and with higher resolution a larger number of grid points are involved in producing this error. At a first glance, the distribution of the relative error with respect to the bed slope unveils larger errors at smaller slopes. However, the distribution is certainly biased by large errors occurring in the fast flowing and smooth trunk of the NEGIS subset (see Fig. 3). By ignoring the bed slope bin from 0 to 0.05 it turns out that higher bed undulations lead to larger errors in the finer resolutions; however, it seems to play a secondary role, compared to e.g. the slip ratio, as less grid nodes are involved. The analysis underlines that the source of stress regime deviations occurs in regions of high slip ratio, high aspect ratio and high topographic variability.

To investigate the effect of FS and BP-like on the overall ice dynamics, the simulated vertical velocities, v_z, influence the internal advection. Figure 8 demonstrates, that differences in the vertical velocity at the surface are apparent (differences for a resolution of 800 m and 6400 m are shown in Fig. A10). For softer ice, the difference is more pronounced and generally located in areas of topographic variability.

5.5 Evaluating the englacial advection

To evaluate the internal ice flow, we compute pathways of particles from the 3D stationary velocity field. Due to the stationary velocity field and the non evolving geometry, the pathways should not be expected to be realistic or even compared to e.g. layers obtained from radio echo sounding; the approach here is just for demonstrating the differences in internal ice flow. However, we

https://doi.org/10.5194/tc-2021-193
Preprint. Discussion started: 16 July 2021

The Cryosphere
Discussions
Open Access
EGU

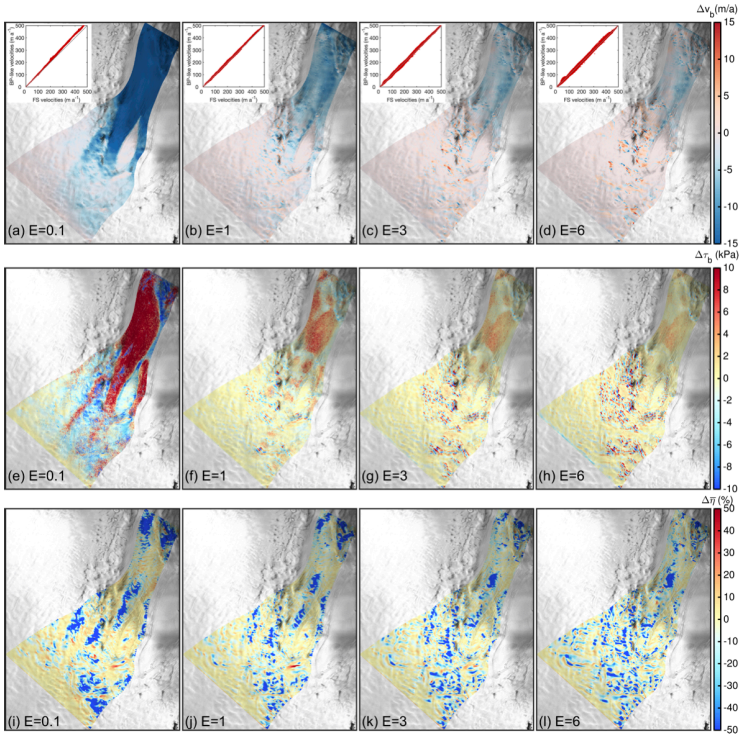

Figure 6. Difference (FS minus BP-like solution) of basal velocities, v_b (a, b, c, d) and basal drag τ_b (e, f, g, h). Relative difference of depth-averaged viscosity $\bar{\eta}$ (i, j, k, l) between FS and BP-like. Differences are shown for a resolution of 100 m. The domain averaged mean viscosities for FS and $E = 0.1$, 1, 3 and 6 are 10.8, 3.6, 1.8, and 1.1×10^{14} Pas, respectively; for BP-like they are 12.6, 4.1, 2.1, and 1.3×10^{14} Pas, respectively. Background image is a RADARSAT Mosaic (Joughin, 2015; Joughin et al., 2016).

seed particles in arbitrary depths at $(x, y) = (350\,\mathrm{km}, -1280\,\mathrm{km})$ and advect them within 3D velocity field through the main ice stream. The pathways taken by the particles are indicated in Fig. 2a. Those pathways are mapped onto the same vertical cross section of the glacier. The individual elevations are not straightforward to compare with each other in this cross-sectional view as particles could use slightly different paths in the horizontal plane (map-plane). However, the paths only differ up to 700 m horizontally.

For the 100 m resolution and the four rheologies, the pathways are displayed in Fig. 9. The particle pathways for $E = 0.1$ generally follow the bed topography, but the FS and BP-like pathway tend to diverge. Pathways with the same seeding location reveal differences in the vertical elevations between FS and BP-like up to 62 m. For $E = 1$, the pattern looks rather similar, but differences of up to 51 m occur mainly around the peak in the bed $(\mathrm{distance} = 60\,\mathrm{km})$ or at pathways closer to the bed.

https://doi.org/10.5194/tc-2021-193
Preprint. Discussion started: 16 July 2021

The Cryosphere Discussions
Open Access
EGU

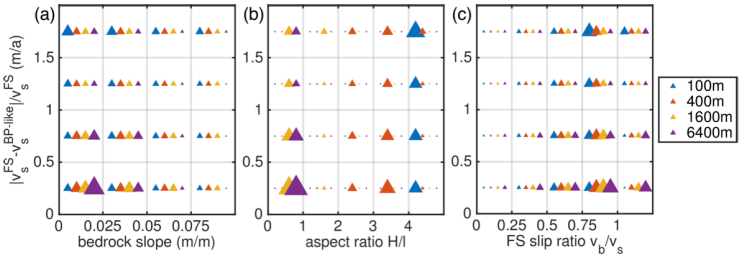

Figure 7. 2D dimensional histograms for $E = 1$ and four different grid resolutions. Counts of grid nodes per relative velocity error bin and per (a) bed slope bin, (b) local aspect ratio bin, and (c) FS slip ratio bin. The sizes of the triangles are normalized by the total number of horizontal grid nodes of each mesh.

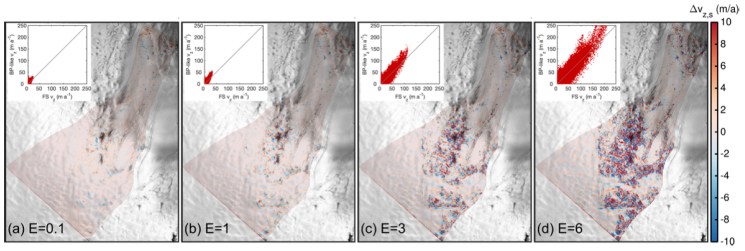

Figure 8. Difference of vertical velocity at the surface $\Delta v_{z,s}^{\text{FS}-\text{BP-like}} = v_{z,s}^{\text{FS}} - v_{z,s}^{\text{BP-like}}$ for a resolution of 100 m. (a, b, c, d) shows differences for $E = 0.1$, 1, 3 and 6, respectively. Background image is a RADARSAT Mosaic (Joughin, 2015; Joughin et al., 2016).

For $E = 3$ and 6, the pathways show large differences in the majority of the vertical flowline and reveal a somewhat chaotic pattern.

Overall, there is no general trend detectable whether FS or BP-like is located below or above each other. Generally, stiffer ice leads to pathways that are located deeper in the ice. This obviously reflects the effect of the differences in vertical velocity discussed above. From these results, a logical consequence would be to let the geometry evolve in order to prove whether the differences are influenced by the fixed topography. However, this is beyond the focus of this study.

A desirable approach would be to compute englacial (age) layers by seeding particles at the surface and track their integration time. However, from the particle pathways, it is obvious that we would not obtain a sufficient depth distribution since surface particles reach a limited depth. Therefore, the retrieved particle pathways merely demonstrate that both flow regimes simulate a different englacial vertical advection scheme in our study. Though not explicitly shown here, it is obvious that these differences would influence the age-depth distribution obtained from, e.g. Lagrangian tracer methods (Sutter et al., 2020). Whether the interpretation for isochrone elevations will fundamentally change by the choice of the stress regimes must be examined further.

https://doi.org/10.5194/tc-2021-193
Preprint. Discussion started: 16 July 2021

However, the expanded view from integrative or, e.g. surface quantities to the englacial 3D flow reveals valuable insights on ice dynamics.

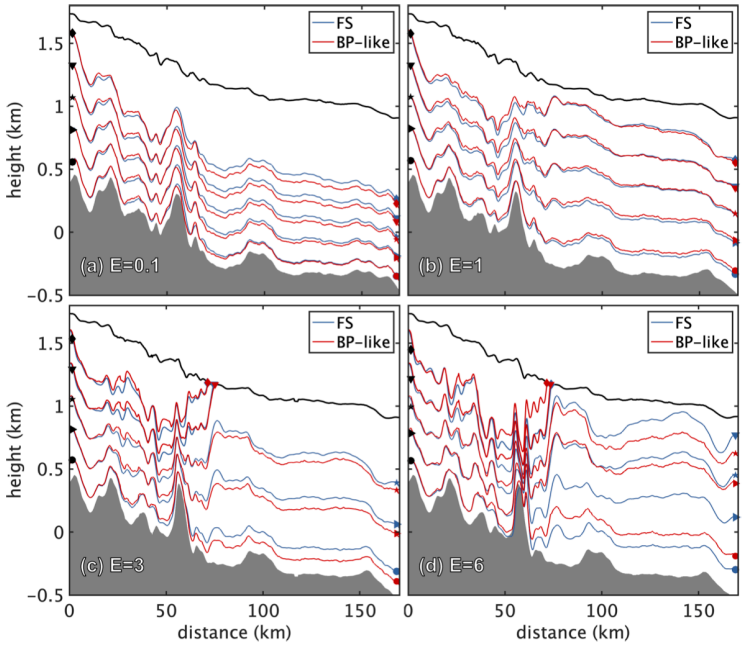

Figure 9. Layering of particle pathways for FS and BP-like along a central flowline for (a) $E = 0.1$, (b) $E = 1$, (c) $E = 3$, and (c) $E = 6$. The coloured symbols indicate the start and end of each pathway. Please note, that some particles are lost as they leave the domain at the surface. The horizontal pathway of the particles is indicated in Fig. 3.

5.6 Impact on ice discharge

To estimate the impact on ice discharge, we calculated the ice mass flux along three flux gates (Fig. 2a). The ice mass flux is calculated as $Q = \int_\Gamma \bar{v} H \varrho_i ds$, where $\bar{v}$ indicates the depth-averaged ice velocity and the usage of the upper case Q indicates integration over the flux gate area Γ with the line segments ds. The location of the three flux gates are (1) in the upper and slow-flowing part, (2) the narrow and fast-flowing part, (3) and at the outflow of our domain. Fig. 10 shows the calculated ice mass fluxes with the four different E values. Generally we observe a progression of differences from the interior towards the outflow of the domain. Largest differences occur for the stiffer ice with up to 8% more ice discharge in the BP-like stress regime; for the classical case up to 3%. With softer ice the differences decrease and fall below $\pm 1\%$ for $E = 6$.

https://doi.org/10.5194/tc-2021-193
Preprint. Discussion started: 16 July 2021

The Cryosphere
Discussions
Open Access
EGU

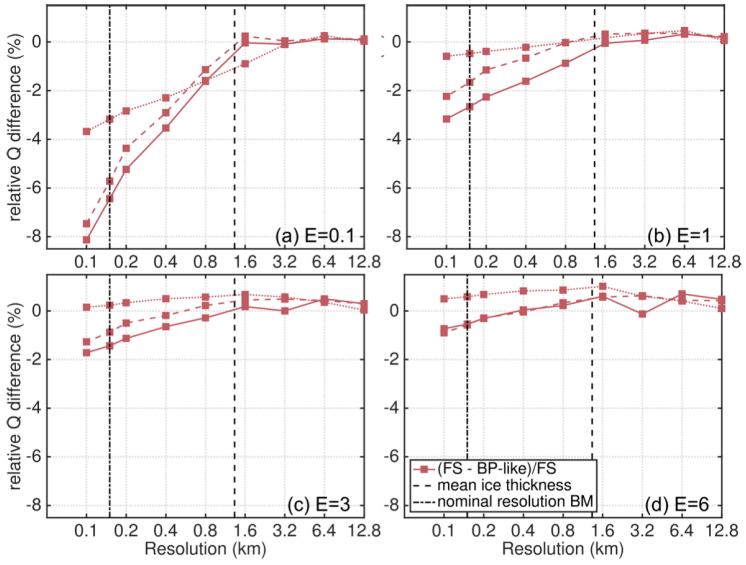

Figure 10. Integrative overview of relative ice mass flux changes between FS and the BP-like stress regimes ($(Q^{\mathrm{FS}} - Q^{\mathrm{BP\text{-}like}})/Q^{\mathrm{FS}}$). The location of the three flux gates is indicated in Fig. 3. On average the total flux at the outflow (straight line) is 15 Gt a^{-1}, at the 'bottleneck' (dashed line) it is 22 Gt a^{-1}, and at the onset area (dotted lines) it is 21 Gt a^{-1}.

6 Discussion

The quantitative comparison of both stress regimes with each other reveals that, particularly in extremes cases ($E = 0.1$ and $E = 6$), the BP-like solution produces higher surface velocities than FS ($E = 0.1$) and a large spread around the FS solution ($E = 6$). However, these extreme cases at such a high resolution are rarely used in the community and can be considered as unrealistic. For the $E = 1$ ('classical case') and $E = 3$, we found distinct differences, but those are very low (about 1.5% in spatially averaged surface velocities). Although these differences are small, they tend to increase further at the highest grid resolution used. We cannot rule out the possibility that a much higher resolution would produce much more substantial disagreements, but a bedrock topography database to investigate this is not available to date. However, since FS is computationally very intensive, it is satisfying to note that the differences between the approximated model and the exact solution are small in resolutions that are currently feasible. Therefore, it might be favourable to use a BP stress regime instead of FS for most glacier modelling studies.

One limitation of our study is that our simulations are not prognostic, i.e. we have not investigated how the solution differences propagate to or interact with other components of an ice sheet model, e.g. by coupling to the ice thickness evolution. The calculation of ice discharge demonstrates that the stress regimes show distinct discrepancies in a key process, but whether

https://doi.org/10.5194/tc-2021-193
Preprint. Discussion started: 16 July 2021

these differences are accumulated in the glaciers mass balance over transient runs, eventually leading to substantially different estimates of ice mass changes, or fading out must be postponed to future studies.

Our numerical experiments are consistent with earlier work. The overestimation of BP-like surface velocities to FS in our study is in agreement with Morlighem et al. (2010). They showed the necessity of a lower basal drag for FS to reproduce observed velocities compared to BP. Similarly, the lower FS ice mass fluxes compared to BP-like supports the tendency that FS contribute less to sea-level rise than simpler models (Seddik et al., 2012; Favier et al., 2014; Seddik et al., 2017).

A process not considered here is the thermo-mechanical coupling. For instance, within a thermo-mechanical coupling, the feedback of temperature on the ice viscosity, in turn, changes the ice flow. However, there are several feasible processes how the stress regime differences can modify the thermal regime: (1) the different representation of the basal drag presumably generates a different amount of frictional heating, (2) the different vertical deformation produces a different internal heat source rate, and (3) the internal advection scheme leads to different heat transport. Though the role of these feedbacks is not explored here, there are indications that small initial differences become much larger over long time integrations (Zhang et al., 2015).

7 Conclusions

We compared two approaches to represent ice flow dynamics, namely the FS and the BP-like formulation, for a subset of the NEGIS ice stream. Both stress regimes are implemented within the same dynamic ice flow model to alleviate a consistent comparison where numerical issues are largely eliminated. Our performed comparison experiments between FS and BP-like stress regimes unveil that BP-like tends to overestimate surface velocities and the resulting ice discharge. This behaviour emerges at a horizontal resolution below the mean ice thickness ($<$1000 m) and continuously increases with finer horizontal resolution (down to 100 m). The model disagreements still tend to diverge below the highest employed horizontal resolution of 100 m. An intriguing effect was identified as much softer ice than currently considered leading to an enhanced spread in surface velocity differences between FS and BP-like. In contrast, ten times stiffer ice leads to an offset in velocities between FS and BP-like with increasing difference towards larger ice flow. Depending on the stiffness of the ice, we identified the basal drag (stiffer ice) and topographic undulations (softer ice) as the general causes for the model disagreements.

Even though differences in the velocity fields are overall minor, a view on particle pathways calculated from both model solutions reveals substantial differences that may influence englacial layering interpretation. It should be proven in further studies whether these discrepancies are relevant over long time integrations as the simplistic estimation performed here is based on a stationary approach.

From the perspective of large scale (centennial) ice sheet projections, FS will start to matter (differences in velocities and ice discharge $\gtrsim$3%) once one can afford resolutions considerably lower than the local ice thickness in faster moving and undulated areas. However, given the huge additional computational amount consumed by FS models and other large uncertainties ice sheet projections (e.g. surface mass balance forcing and other boundary conditions that have a larger impact on ice sheet evolution), the use of FS seems not an urgent issue.

https://doi.org/10.5194/tc-2021-193
Preprint. Discussion started: 16 July 2021

The Cryosphere Discussions
Open Access
EGU

Code and data availability. COMSOL Multiphysics© is a commercial software and not freely available. The models used here are accessible for COMSOL users upon request to the authors. The ice flow model ISSM is open source and freely available at https://issm.jpl.nasa.gov/ (last access: July 15, 2021; (Larour et al., 2012). Simulation results will be made accessible through the World Data Center PANGAEA (https://doi.pangaea.de/XXX).

.

Appendix A: Inversion with ISSM

The simulations presented make use of a basal friction coefficient, k^2, that is inferred by an inversion method. For the inversion of the basal friction coefficient, we operate the Ice-Sheet and Sea-level System Model (ISSM, Morlighem et al., 2010; Larour et al., 2012), an open source finite element flow model appropriate for continental-scale and outlet glacier applications. The setup is as described above, i.e. (1) domain outline and geometry data set is similar as in the COMSOL simulations (see Fig. 2), (2) ice rheology is taken from SICOPOLIS spinup (Rückamp et al., 2019) and interpolated onto the computational mesh and (3) the friction law follows the form in Eq. 6. But for the ease of computational time model calculations are performed on a structured finite element grid with a horizontal resolution of 1 km and the BP-stress regime. The inversion is conducted separately for each enhancement factor $E = 0.1$, 1, 3 and 6.

Within the inverse problem a cost function (J), that measures the misfit between observed, $\mathbf{v}^{\mathrm{obs}} = (v_x^{\mathrm{obs}}, v_y^{\mathrm{obs}})$, and simulated velocities, $\mathbf{v} = (v_{\mathrm{y}}, v_{\mathrm{y}})$, is minimized. We use the observed velocities from the MEaSUREs project (Joughin et al., 2016, 2018) as target within the inversion. The cost function is composed of two terms which fit the velocities in fast- and slow-moving areas. A third term is a Tikhonov regularization to avoid oscillations due to over fitting. The cost function is defined as follows:

$$J(\mathbf{v},k) = \gamma_1 \frac{1}{2}\int_{\Gamma_s} (v_x - v_y^{\mathrm{obs}})^2 + v_y - v_y^{\mathrm{obs}})^2 d\Gamma_s + \gamma_2 \frac{1}{2}\int_{\Gamma_s} \ln\left(\frac{\sqrt{v_x^2+v_y^2}+\varepsilon}{\sqrt{{v_x^{\mathrm{obs}}}^2+{v_y^{\mathrm{obs}}}^2}+\varepsilon}\right)^2 d\Gamma_s + \gamma_t \frac{1}{2}\int_{\Gamma_b} \nabla k \cdot \nabla k \, d\Gamma_b, \qquad \text{(A1)}$$

where ε is a minimum velocity used to avoid singularities and Γ_s and Γ_b are the ice surface and ice base, respectively. An L-curve analysis was performed to pick the Tikhonov parameter γ_t (not shown). We obtained a good agreement to the observed velocities by choosing with $\gamma_1 = 1 \times 10^3$, $\gamma_2 = 1 \times 10^4$ and $\gamma_t = 1 \times 10^{-4}$ (see Fig. A1).

https://doi.org/10.5194/tc-2021-193
Preprint. Discussion started: 16 July 2021

The Cryosphere
Discussions
Open Access
EGU

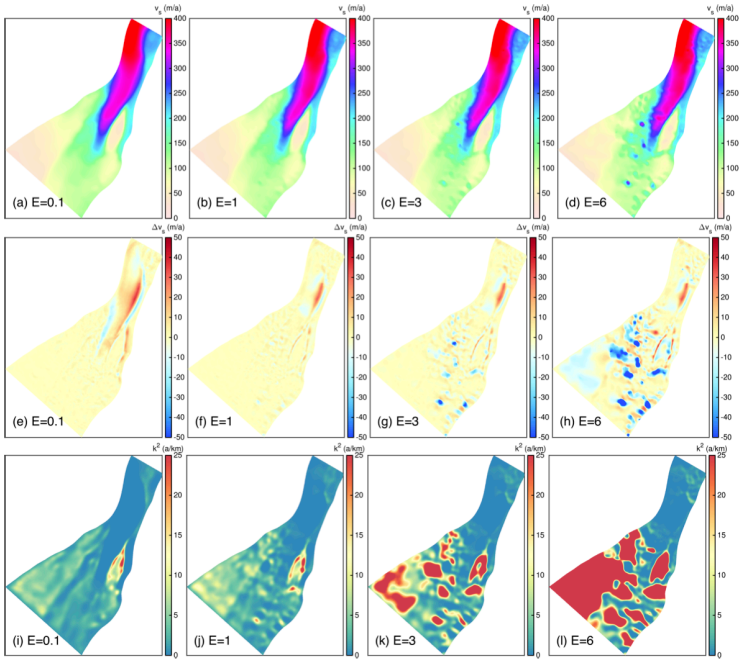

Figure A1. Overview of the ISSM inversion performed with the different values for $E = 0.1$, 1, 3 and 6. (a, b, c, d) Simulated surface velocities. (e, f, g, h). Velocity difference between observed and simulated velocities. (i, j, k, l) Inferred basal friction coefficient k^2.

https://doi.org/10.5194/tc-2021-193
Preprint. Discussion started: 16 July 2021

The Cryosphere
Discussions
Open Access
EGU

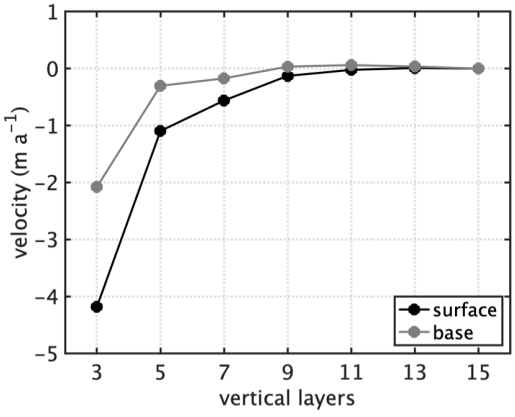

Figure A2. Surface and basal area-averaged velocity for different numbers of vertical layers. Velocity is presented relative to simulation results obtained with 15 vertical layers. Results are shown for $E = 1$, employed FS regime and a horizontal resolution of $l = 400\,\mathrm{m}$.

https://doi.org/10.5194/tc-2021-193
Preprint. Discussion started: 16 July 2021

The Cryosphere
Discussions
Open Access
EGU

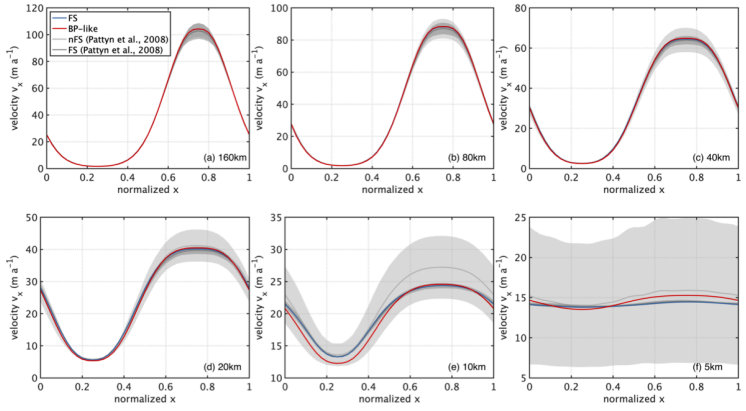

Figure A3. Results of ISMIP-HOM benchmark Exp. A. Surface velocity component v_x (m a^{-1}) across the bump at $y = L/4$ for different length scales, with L ranging from 160 to 5 km. Values computed in the study for FS and BP-like are compared to results by simpler models (nFS) and FS from the ISMIP-HOM benchmark (Pattyn et al., 2008).

https://doi.org/10.5194/tc-2021-193
Preprint. Discussion started: 16 July 2021

The Cryosphere
Discussions
Open Access
EGU

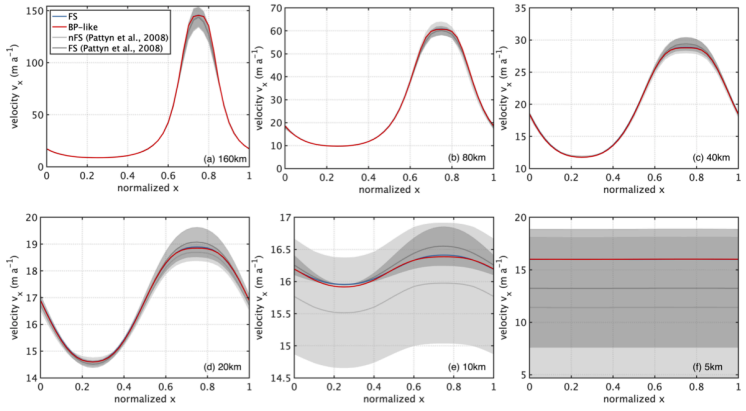

Figure A4. Results of ISMIP-HOM benchmark Exp. C. Surface velocity component v_x (m a^{-1}) across the bump at $y = L/4$ for different length scales, with L ranging from 160 to 5 km. Values computed in the study for FS and BP-like are compared to results by simpler models (nFS) and FS from the ISMIP-HOM benchmark (Pattyn et al., 2008).

https://doi.org/10.5194/tc-2021-193
Preprint. Discussion started: 16 July 2021

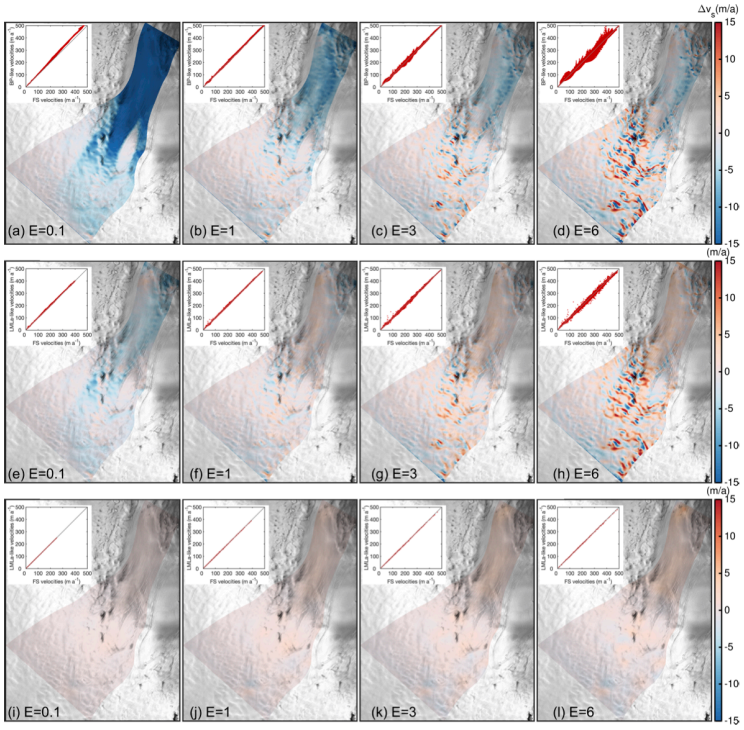

Figure A5. Difference of surface velocity $\Delta v_s^{\mathrm{FS-BP\text{-}like}} = v_s^{\mathrm{FS}} - v_s^{\mathrm{BP\text{-}like}}$ for a resolution of 100 m (a–d), 800 m (e–h), and 6400 m (i–l). Each column shows differences for $E = 0.1$, 1, 3 and 6, respectively. Background image is a RADARSAT Mosaic (Joughin, 2015; Joughin et al., 2016).

https://doi.org/10.5194/tc-2021-193
Preprint. Discussion started: 16 July 2021

The Cryosphere Discussions
Open Access
EGU

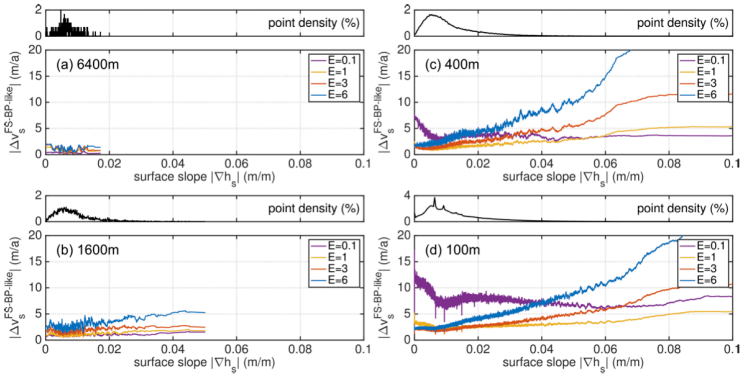

Figure A6. Line plots of the absolute surface velocity difference between FS and BP-like ($|\Delta v_s^{\text{FS-BP-like}}|$) versus the surface slope for a resolution of $l = 6400$ m (a), a resolution of $l = 1600$ m (b), a resolution of $l = 400$ m (c), and a resolution of $l = 100$ m (d). A moving mean with a window of 2500 data points is applied.

https://doi.org/10.5194/tc-2021-193
Preprint. Discussion started: 16 July 2021

The Cryosphere
Discussions
Open Access
EGU

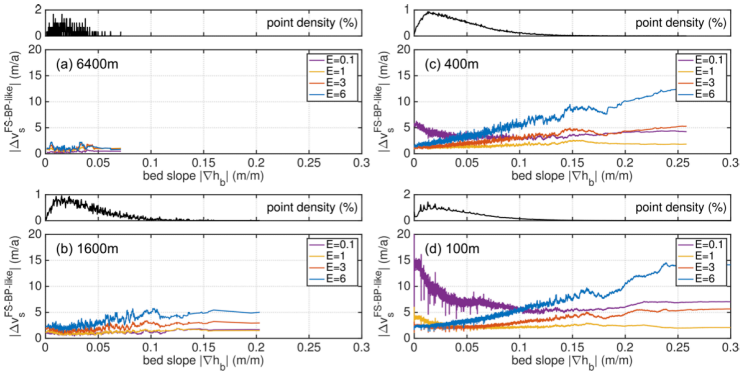

Figure A7. Line plots of the absolute surface velocity difference between FS and BP-like ($|\Delta v_s^{\text{FS-BP-like}}|$) versus the bed slope for a resolution of $l = 6400$ m (a), a resolution of $l = 1600$ m (b), a resolution of $l = 400$ m (c), and a resolution of $l = 100$ m (d). A moving mean with a window of 2500 data points is applied.

https://doi.org/10.5194/tc-2021-193
Preprint. Discussion started: 16 July 2021

The Cryosphere
Discussions
Open Access
EGU

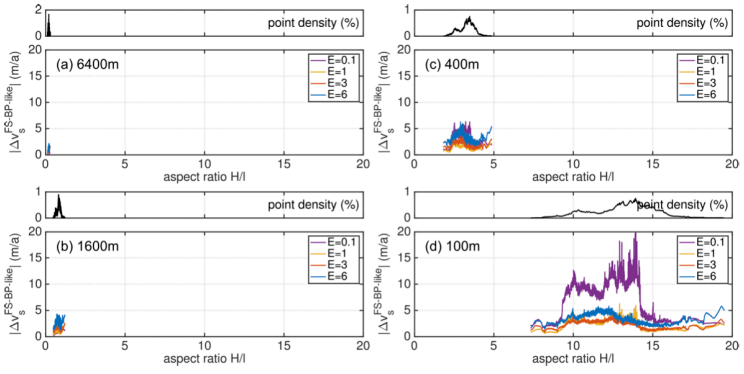

Figure A8. Line plots of the absolute surface velocity difference between FS and BP-like ($|\Delta v_s^{\text{FS-BP-like}}|$) versus the local aspect ratio for a resolution of $l = 6400$ m (a), a resolution of $l = 1600$ m (b), a resolution of $l = 400$ m (c), and a resolution of $l = 100$ m (d). A moving mean with a window of 2500 data points is applied.

https://doi.org/10.5194/tc-2021-193
Preprint. Discussion started: 16 July 2021

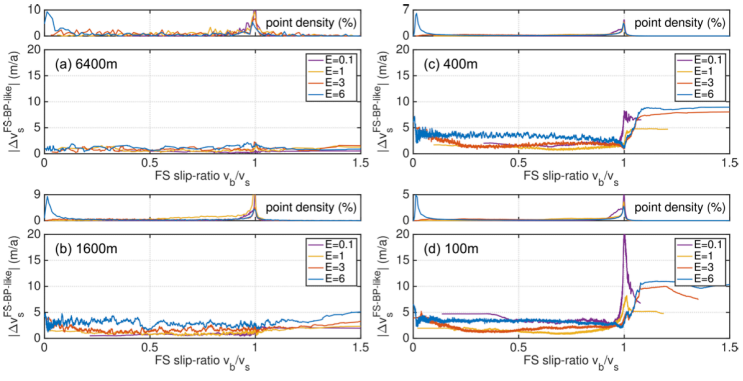

Figure A9. Line plots of the absolute surface velocity difference between FS and BP-like ($|\Delta v_s^{\text{FS-BP-like}}|$) versus the FS slip ratio (v_b/v_s) for a resolution of $l = 6400$ m (a), a resolution of $l = 1600$ m (b), a resolution of $l = 400$ m (c), and a resolution of $l = 100$ m (d). A moving mean with a window of 2500 data points is applied.

https://doi.org/10.5194/tc-2021-193
Preprint. Discussion started: 16 July 2021

The Cryosphere
Discussions
Open Access
EGU

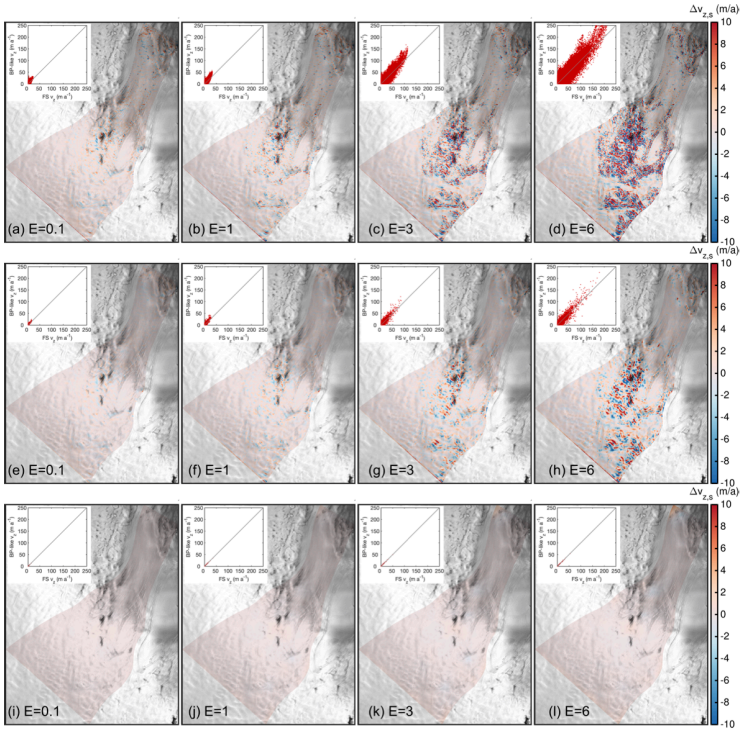

Figure A10. Difference of vertical velocity at the surface $\Delta v_{z,s}^{\text{FS}-\text{BP-like}} = v_{z,s}^{\text{FS}} - v_{z,s}^{\text{BP-like}}$ for a resolution of 100 m (a–d), 800 m (e–h), and 6400 m (i–l). Each column shows differences for $E = 0.1$, 1, 3 and 6, respectively. Background image is a RADARSAT Mosaic (Joughin, 2015; Joughin et al., 2016).

Author contributions. MR setup the COMSOL FS and BP model and the ISSM model, conducted the simulation and wrote large parts of the manuscript. AH designed the study. MR, TK and AH analyzed the results. All author contributed in writing the manuscript.

Competing interests. The authors declare that they have no conflict of interest.

Acknowledgements. The simulations were performed at AWI's cluster Cray-CS400 and at the North-German Supercomputing Alliance (HLRN). We would like to thank Natalja Rakowsky (AWI) for providing excellent support for COMSOL at computing facilities at AWI and

https://doi.org/10.5194/tc-2021-193
Preprint. Discussion started: 16 July 2021

HLRN. Ralf Greve (ILTS) kindly provided results from spin-up simulations with SICOPOLIS. We thank Eberhard Bänsch and Luca Wester for discussions on Stokes simulations (both Friedrich-Alexander-University of Erlangen).

https://doi.org/10.5194/tc-2021-193
Preprint. Discussion started: 16 July 2021

References

Ahlkrona, J., Kirchner, N., and Lötstedt, P.: Accuracy of the zeroth- and second-order shallow-ice approximation – numerical and theoretical results, Geoscientific Model Development, 6, 2135–2152, https://doi.org/10.5194/gmd-6-2135-2013, 2013.

Aschwanden, A., Fahnestock, M. A., Truffer, M., Brinkerhoff, D. J., Hock, R., Khroulev, C., Mottram, R., and Khan, S. A.: Contribution of the Greenland Ice Sheet to sea level over the next millennium, Science Advances, 5, https://doi.org/10.1126/sciadv.aav9396, 2019.

Blatter, H.: Velocity and stress fields in grounded glaciers: a simple algorithm for including deviatoric stress gradients, Journal of Glaciology, 41, 333–344, https://doi.org/10.3189/S002214300001621X, 1995.

Born, A.: Tracer transport in an isochronal ice-sheet model, Journal of Glaciology, 63, 22–38, https://doi.org/10.1017/jog.2016.111, 2017.

Budd, W. F., Keage, P. L., and Blundy, N. A.: Empirical Studies of Ice Sliding, Journal of Glaciology, 23, 157–170, https://doi.org/10.3189/S0022143000029804, 1979.

Bueler, E. and Brown, J.: Shallow shelf approximation as a "sliding law" in a thermodynamically coupled ice sheet model, J. Geophys. Res., 114, https://doi.org/10.1029/2008JF001179, 2009.

Cornford, S. L., Seroussi, H., Asay-Davis, X. S., Gudmundsson, G. H., Arthern, R., Borstad, C., Christmann, J., Dias dos Santos, T., Feldmann, J., Goldberg, D., Hoffman, M. J., Humbert, A., Kleiner, T., Leguy, G., Lipscomb, W. H., Merino, N., Durand, G., Morlighem, M., Pollard, D., Rückamp, M., Williams, C. R., and Yu, H.: Results of the third Marine Ice Sheet Model Intercomparison Project (MISMIP+), The Cryosphere, 14, 2283–2301, https://doi.org/10.5194/tc-14-2283-2020, 2020.

Cuffey, K. M. and Paterson, W. S. B.: The Physics of Glaciers, Elsevier, Amsterdam, The Netherlands etc., 4th edn., 2010.

Favier, L., Durand, G., Cornford, S. L., Gudmundsson, G. H., Gagliardini, O., Gillet-Chaulet, F., Zwinger, T., Payne, A., and Le Brocq, A. M.: Retreat of Pine Island Glacier controlled by marine ice-sheet instability, Nature Climate Change, 4, 117–121, https://doi.org/10.1038/NCLIMATE2094, 2014.

Glen, J. W.: The Creep of Polycrystalline Ice, Proceedings of the Royal Society of London. Series A, Mathematical and Physical Sciences, 228, 519–538, https://doi.org/10.1098/rspa.1955.0066, 1955.

Goelzer, H., Nowicki, S., Edwards, T., Beckley, M., Abe-Ouchi, A., Aschwanden, A., Calov, R., Gagliardini, O., Gillet-Chaulet, F., Golledge, N. R., Gregory, J., Greve, R., Humbert, A., Huybrechts, P., Kennedy, J. H., Larour, E., Lipscomb, W. H., Le clec'h, S., Lee, V., Morlighem, M., Pattyn, F., Payne, A. J., Rodehacke, C., Rückamp, M., Saito, F., Schlegel, N., Seroussi, H., Shepherd, A., Sun, S., van de Wal, R., and Ziemen, F. A.: Design and results of the ice sheet model initialisation experiments initMIP-Greenland: an ISMIP6 intercomparison, The Cryosphere, 12, 1433–1460, https://doi.org/10.5194/tc-12-1433-2018, 2018.

Goelzer, H., Nowicki, S., Payne, A., Larour, E., Seroussi, H., Lipscomb, W. H., Gregory, J., Abe-Ouchi, A., Shepherd, A., Simon, E., Agosta, C., Alexander, P., Aschwanden, A., Barthel, A., Calov, R., Chambers, C., Choi, Y., Cuzzone, J., Dumas, C., Edwards, T., Felikson, D., Fettweis, X., Golledge, N. R., Greve, R., Humbert, A., Huybrechts, P., Le clec'h, S., Lee, V., Leguy, G., Little, C., Lowry, D. P., Morlighem, M., Nias, I., Quiquet, A., Rückamp, M., Schlegel, N.-J., Slater, D. A., Smith, R. S., Straneo, F., Tarasov, L., van de Wal, R., and van den Broeke, M.: The future sea-level contribution of the Greenland ice sheet: a multi-model ensemble study of ISMIP6, The Cryosphere, 14, 3071–3096, https://doi.org/10.5194/tc-14-3071-2020, 2020.

Gudmundsson, G. H.: Transmission of basal variability to a glacier surface, Journal of Geophysical Research: Solid Earth, 108, 2253, https://doi.org/10.1029/2002JB002107, 2003.

Hauke, G. and Hughes, T.: A unified approach to compressible and incompressible flows, Computer Methods in Applied Mechanics and Engineering, 113, 389–395, https://doi.org/10.1016/0045-7825(94)90055-8, 1994.

https://doi.org/10.5194/tc-2021-193
Preprint. Discussion started: 16 July 2021

Hindmarsh, R. C. A.: A numerical comparison of approximations to the Stokes equations used in ice sheet and glacier modeling, Journal of Geophysical Research: Earth Surface, 109, https://doi.org/10.1029/2003JF000065, 2004.

Hutter, K.: Theoretical glaciology : material science of ice and the mechanics of glaciers and ice sheets, Reidel/Terra Pub. Co., Dordrecht, 1983.

Huybrechts, P.: The Antarctic ice sheet and environmental change: a three-dimensional modelling study = Der antarktische Eisschild und globale Umweltveränderungen : eine dreidimensionale Modellstudie, https://doi.org/10.2312/BzP_0099_1992, 1992.

IPCC: Climate Change 2013: The Physical Science Basis. Contribution of Working Group I to the Fifth Assessment Report of the Intergovernmental Panel on Climate Change, Cambridge University Press, Cambridge, United Kingdom and New York, NY, USA, https://doi.org/10.1017/CBO9781107415324, 2013.

Joughin, I.: MEaSUREs Greenland Ice Sheet Mosaics from SAR Data, Version 1. Boulder, Colorado USA. NASA National Snow and Ice Data Center Distributed Active Archive Center, https://doi.org/10.5067/6187DQUL3FR5, 2015.

Joughin, I., Smith, B. E., Howat, I. M., Moon, T., and Scambos, T. A.: A SAR record of early 21st century change in Greenland, Journal of Glaciology, 62, 62–71, https://doi.org/10.1017/jog.2016.10, 2016.

Joughin, I., Smith, B. E., and Howat, I. M.: A complete map of Greenland ice velocity derived from satellite data collected over 20 years, Journal of Glaciology, 64, 1–11, https://doi.org/10.1017/jog.2017.73, 2018.

Larour, E., Seroussi, H., Morlighem, M., and Rignot, E.: Continental scale, high order, high spatial resolution, ice sheet modeling using the Ice Sheet System Model (ISSM), Journal of Geophysical Research, 117, F01 022, https://doi.org/10.1029/2011JF002140, 2012.

Le Meur, E., Gagliardini, O., Zwinger, T., and Ruokolainen, J.: Glacier flow modelling: a comparison of the Shallow Ice Approximation and the full-Stokes solution, Comptes Rendus Physique, 5, 709–722, https://doi.org/https://doi.org/10.1016/j.crhy.2004.10.001, ice: from dislocations to icy satellites, 2004.

Leysinger Vieli, G. J.-M. C. and Gudmundsson, G. H.: On estimating length fluctuations of glaciers caused by changes in climatic forcing, Journal of Geophysical Research: Earth Surface, 109, https://doi.org/10.1029/2003JF000027, 2004.

Lliboutry, L. and Duval, P.: Various isotropic and anisotropic ices found in glaciers and polar ice caps and their corresponding rheologies, Annales Geophysicae, 3, 207–224, 1985.

Morlighem, M., Rignot, E., Seroussi, H., Larour, E., Dhia, H., and Aubry, D.: Spatial patterns of basal drag inferred using control methods from a full-Stokes and simpler models for Pine Island Glacier, West Antarctica, Geophysical Research Letters, 37, L14 502, 2010.

Morlighem, M., Williams, C. N., Rignot, E., An, L., Arndt, J. E., Bamber, J. L., Catania, G., Chauché, N., Dowdeswell, J. A., Dorschel, B., Fenty, I., Hogan, K., Howat, I., Hubbard, A., Jakobsson, M., Jordan, T. M., Kjeldsen, K. K., Millan, R., Mayer, L., Mouginot, J., Noël, B. P. Y., O'Cofaigh, C., Palmer, S., Rysgaard, S., Seroussi, H., Siegert, M. J., Slabon, P., Straneo, F., van den Broeke, M. R., Weinrebe, W., Wood, M., and Zinglersen, K. B.: BedMachine v3: Complete bed topography and ocean bathymetry mapping of Greenland from multibeam echo sounding combined with mass conservation, Geophysical Research Letters, 44, 11 051–11 061, https://doi.org/10.1002/2017GL074954, 2017.

Nowicki, S. M. J., Payne, A., Larour, E., Seroussi, H., Goelzer, H., Lipscomb, W., Gregory, J., Abe-Ouchi, A., and Shepherd, A.: Ice Sheet Model Intercomparison Project (ISMIP6) contribution to CMIP6, Geoscientific Model Development, 9, 4521–4545, https://doi.org/10.5194/gmd-9-4521-2016, 2016.

Oppenheimer, M., Glavovic, B., Hinkel, J., van de Wal, R., Magnan, A., Abd-Elgawad, A., Cai, R., Cifuentes-Jara, M., Deconto, R., Ghosh, T., et al.: Sea level rise and implications for low-lying islands, coasts and communities IPCC Special Report on the Ocean and Cryosphere in a Changing Climate ed HO Pörtner et al, 2019.

https://doi.org/10.5194/tc-2021-193
Preprint. Discussion started: 16 July 2021

Pattyn, F.: A new three-dimensional higher-order thermomechanical ice-sheet model: basic sensitivity, ice-stream development and ice flow across subglacial lakes, Journal of Geophysical Research, 108, 2382, https://doi.org/10.1029/2002JB002329, 2003.

Pattyn, F., Perichon, L., Aschwanden, A., Breuer, B., de Smedt, B., Gagliardini, O., Gudmundsson, G. H., Hindmarsh, R. C. A., Hubbard, A., Johnson, J. V., Kleiner, T., Konovalov, Y., Martin, C., Payne, A. J., Pollard, D., Price, S., Rückamp, M., Saito, F., Souček, O., Sugiyama, S., and Zwinger, T.: Benchmark experiments for higher-order and full-Stokes ice sheet models (ISMIP-HOM), The Cryosphere, 2, 95–108, https://doi.org/10.5194/tc-2-95-2008, 2008.

Pattyn, F., Schoof, C., Perichon, L., Hindmarsh, R. C. A., Bueler, E., de Fleurian, B., Durand, G., Gagliardini, O., Gladstone, R., Goldberg, D., Gudmundsson, G. H., Huybrechts, P., Lee, V., Nick, F. M., Payne, A. J., Pollard, D., Rybak, O., Saito, F., and Vieli, A.: Results of the Marine Ice Sheet Model Intercomparison Project, MISMIP, The Cryosphere, 6, 573–588, https://doi.org/10.5194/tc-6-573-2012, 2012.

Pattyn, F., Perichon, L., Durand, G., Favier, L., Gagliardini, O., Hindmarsh, R., Zwinger, T., Albrecht, T., Cornford, S., Docquier, D., Fürst, J. J., Goldberg, D., Gudmundsson, G. H., Humbert, A., Hütten, M., Huybrechts, P., Jouvet, G., Kleiner, T., Larour, E., Martin, D., Morlighem, M., Payne, A. J., Pollard, D., Rückamp, M., Rybak, O., Seroussi, H., Thoma, M., and Wilkens, N.: Grounding-line migration in plan-view marine ice-sheet models: results of the ice2sea MISMIP3d intercomparison, Journal of Glaciology, 59, 410–422, https://doi.org/doi:10.3189/2013JoG12J129, 2013.

Rückamp, M., Greve, R., and Humbert, A.: Comparative simulations of the evolution of the Greenland ice sheet under simplified Paris Agreement scenarios with the models SICOPOLIS and ISSM, Polar Science, 21, 14–25, https://doi.org/10.1016/j.polar.2018.12.003, 2019.

Saad, Y.: Iterative Methods for Sparse Linear System, Philadelphia, PA, USA: Society for Industrial and Applied Mathematics, 2003.

Seddik, H., Greve, R., Zwinger, T., Gillet-Chaulet, F., and Gagliardini, O.: Simulations of the Greenland ice sheet 100 years into the future with the full Stokes model Elmer/Ice, Journal of Glaciology, 58, 427–440, https://doi.org/10.3189/2012JoG11J177, 2012.

Seddik, H., Greve, R., Zwinger, T., and Sugiyama, S.: Regional modeling of the Shirase drainage basin, East Antarctica: full Stokes vs. shallow ice dynamics, The Cryosphere, 11, 2213–2229, https://doi.org/10.5194/tc-11-2213-2017, 2017.

Seroussi, H., Nowicki, S., Simon, E., Abe-Ouchi, A., Albrecht, T., Brondex, J., Cornford, S., Dumas, C., Gillet-Chaulet, F., Goelzer, H., Golledge, N. R., Gregory, J. M., Greve, R., Hoffman, M. J., Humbert, A., Huybrechts, P., Kleiner, T., Larour, E., Leguy, G., Lipscomb, W. H., Lowry, D., Mengel, M., Morlighem, M., Pattyn, F., Payne, A. J., Pollard, D., Price, S. F., Quiquet, A., Reerink, T. J., Reese, R., Rodehacke, C. B., Schlegel, N.-J., Shepherd, A., Sun, S., Sutter, J., Van Breedam, J., van de Wal, R. S. W., Winkelmann, R., and Zhang, T.: initMIP-Antarctica: an ice sheet model initialization experiment of ISMIP6, The Cryosphere, 13, 1441–1471, https://doi.org/10.5194/tc-13-1441-2019, 2019.

Seroussi, H., Nowicki, S., Payne, A. J., Goelzer, H., Lipscomb, W. H., Abe-Ouchi, A., Agosta, C., Albrecht, T., Asay-Davis, X., Barthel, A., Calov, R., Cullather, R., Dumas, C., Galton-Fenzi, B. K., Gladstone, R., Golledge, N. R., Gregory, J. M., Greve, R., Hattermann, T., Hoffman, M. J., Humbert, A., Huybrechts, P., Jourdain, N. C., Kleiner, T., Larour, E., Leguy, G. R., Lowry, D. P., Little, C. M., Morlighem, M., Pattyn, F., Pelle, T., Price, S. F., Quiquet, A., Reese, R., Schlegel, N.-J., Shepherd, A., Simon, E., Smith, R. S., Straneo, F., Sun, S., Trusel, L. D., Van Breedam, J., van de Wal, R. S. W., Winkelmann, R., Zhao, C., Zhang, T., and Zwinger, T.: ISMIP6 Antarctica: a multi-model ensemble of the Antarctic ice sheet evolution over the 21st century, The Cryosphere, 14, 3033–3070, https://doi.org/10.5194/tc-14-3033-2020, 2020.

Steinemann, S.: Results of Preliminary Experiments on the Plasticity of Ice Crystals, Journal of Glaciology, 2, 404–416, https://doi.org/10.3189/002214354793702533, 1954.

https://doi.org/10.5194/tc-2021-193
Preprint. Discussion started: 16 July 2021

Sutter, J., Fischer, H., and Eisen, O.: Simulating the internal structure of the Antarctic Ice Sheet – towards a spatio-temporal calibration for ice-sheet modelling, The Cryosphere Discussions, 2020, 1–25, https://doi.org/10.5194/tc-2020-349, 2020.

Widlund, O. and Toselli, A.: Domain decomposition methods - algorithms and theory, vol. 34 of *Springer Series in Computational Mathematics*, Springer, 2005.

Wilkens, N., Behrens, J., Kleiner, T., Rippin, D., Rückamp, M., and Humbert, A.: Thermal structure and basal sliding parametrisation at Pine Island Glacier - a 3-D full-Stokes model study, The Cryosphere, 9, 675–690, https://doi.org/10.5194/tc-9-675-2015, 2015.

Zhang, T., Ju, L., Leng, W., Price, S., and Gunzburger, M.: Thermomechanically coupled modelling for land-terminating glaciers: a comparison of two-dimensional, first-order and three-dimensional, full-Stokes approaches, Journal of Glaciology, 61, 702–712, https://doi.org/10.3189/2015JoG14J220, 2015.